DCM Modulation: A Three-Axis Rotation Stabilization Technique for Bipedal Locomotion Control

Yuichi Tazaki†

***Abstract*— This paper proposes a simple controller for bipedal locomotion that can stabilize three-axis (roll, pitch, and yaw) rotation without relying on ground reaction moment manipulation. Extra acceleration of the CoM (center-of-mass) from the nominal DCM (divergent component of motion) dynamics generates moment around the CoM. Based on this principle, the behavior of the desired DCM is modulated to carry signal for rotation stabilization. A robust walking controller is synthesized by combining the proposed rotation stabilizer with continuous step adaptation. Simulation study shows that the proposed controller is capable of robust disturbance rejection and yaw-regulated walking of a point-foot robot.**

I. Introduction

A. Need for Simple Model-based Balance Control

Maintaining balance using limited support is one of the fundamental functionalities of humanoid robots that can work in real environments. Unlike quadruped and other multipeds that can create stable support regions using three or more simultaneous contacts, bipedal robots including humanoids need to balance on only two feet with limited support area. Because of this fact, balance control of bipedal robots has attracted tremendous research effort for decades and remains challenging even today.

Recent years have seen significant advances of data-driven approaches to locomotion controller synthesis that can realize robust walking on rough and unmodeled terrain. However, pure end-to-end learning is known to require massive amount of training data, and interpretation of acquired control mechanism is difficult. To reduce the cost of training, utilizing a model-based controller as a priori knowledge for bootstrapping training has been actively investigated [1]. Model-based approaches to controller design directly based on physical principle of bipedal locomotion will therefore continue to attract both theoretical and practical interest.

B. Review of Existing Balance Control Methods

Balance control strategy of human is categorized into ankle, hip, and stepping strategies. From a control theoretic perspective, the ankle strategy is stabilization of the CoM by manipulating the ZMP (zero tilting-moment point). Although the ZMP can easily be manipulated by using the ankle joint torque, stability margin created by this strategy alone is limited because the ZMP is restricted inside the support region. The hip strategy is interpreted as utilization of angular momentum variation for expanding the stability margin of the CoM [2, 3, 4, 5, 6, 7, 8] (more detailed discussion follows in the next subsection). The stepping strategy is adjustment of the placement of footsteps to absorb the perturbation of the CoM. Two types of step adaptation methods have been investigated: step-to-step and continuous. Step-to-step methods determine the next foot placement every time the swing foot touches down [9, 10, 11]. An advantage of this approach is that it can be combined with well-studied capturability theory to realize multi-step prediction. Its drawback is that recovery action againt disturbances applied during the single support phase has to be delayed until the next support exchange. On the other hand, continuous methods monitor the centroidal state continuously during the swing phase and adjust the next foot placement based on the desired DCM offset at touch down [12, 13, 14]. Thanks to its continuous nature, this method can swiftly respond to disturbances applied at arbitrary timing. Recent studies realized complex step adaptation considering crossing of legs [15] and restriction of support regions [16]. Apart from the above three strategies, utilizing variation of the CoM height to expand the stabilizable margin has been investigated in several studies [17, 18, 19, 5, 20, 7].

C. Treatment of Angular Momentum in Balance Control

As mentioned earlier, the most widely accepted way to utilize angular momentum in balance control is to treat it as extra control input to expand the stabilizable margin of the CoM. For this purpose, the notion of Centroidal Moment Pivot (CMP) [21] and eCMP [22] has been used as an extension of the coventional ZMP. That is, the CMP can be set outside the support region to generate greater lateral acceleration of the CoM. The resultant angular momentum variation is often considered as a side-effect.

Another way is to treat it as disturbance caused by the nonlinearity of whole-body motion [23, 24, 25]. The rate of change of angular momentum term is integrated into the CoM dynamics to compensate for the nonlinear effect.

Yet another way, which is quite different from the other two, is to view angular momentum regulation as a primary objective and utilize extra acceleration of the CoM to generate recovery moment to regulate the angular momentum. Pioneering works in this direction are Nagasaka's Body Compliance Control [26] and Takenaka's Model ZMP Control [27], but unfortunately, this approach seems to be less recognized in the research community. The author believes combining this approach with modern continuous step adaptation techniques can realize a simple yet robust balance controller.

†The author is with Faculty of Engineering, Department of Mechanical Engineering, University of Kobe, 1-1 Rokkodai, Nada-ku, Kobe, Japan. tazaki@mech.kobe-u.ac.jp

Lastly, coupling of yaw rotation and CoM movement has long been recognized but poorly studied, because yaw moment generated by CoM movement can be naturally cancelled by torsional friction moment assuming strong enough grip between the support foot and the ground. In case of low ground friction and small support area, however, it could cause slipping of the support foot and instability of walking. Controlling yaw rotation by means of CoM movement is therefore an important topic to explore.

D. Contribution of This Paper

The main goal of this study is to reformulate the idea of stabilizing body rotation by extra horizontal CoM acceleration based on the modern DCM-based theoretical foundation and further extend it to enable yaw regulation. Concrete contributions are summarized as follows.

- The relationship between angular momentum variation and deviation of the DCM from the nominal DCM dynamics is derived. Based on this knowledge, a simple feedback control law that regulates roll, pitch, and yaw rotation without using ground reaction moment is presented.
- A simple and robust bipedal walking controller that combines the proposed rotation stabilizer and continuous step adaptation strategy is developed.
- The performance of the proposed controller is evaluated in dynamical simulation including yaw-regulated walking of a point-foot robot.

The organization of this paper is as follows. In Section II, the relationship between the angular momentum and the linear CoM movement is reviewed, and in Section III, a control method based on this principle is presented. In Section IV, the proposed controller is evaluated in dynamical simulation. Concluding remarks are given in Section V.

II. Analysis on the Relationship between Rotational and the DCM Dynamics

We start from the well-known centroidal dynamics equation, which describes the relationship between the linear and angular momenta and the contact wrench.

$$m\ddot{\boldsymbol{p}} = \boldsymbol{f} - m\boldsymbol{g}, \tag{1a}$$

$$\dot{\boldsymbol{L}} = \boldsymbol{e}_{\mathrm{z}}\eta - (\boldsymbol{p}-\boldsymbol{c}) \times \boldsymbol{f} \tag{1b}$$

Here, m is the total mass, $\boldsymbol{g}$ is the acceleration of gravity, $\boldsymbol{p}$ is the center of mass (CoM), and $\boldsymbol{L}$ is the angular momentum. Moreover, the zero tilting-moment point (ZMP) $\boldsymbol{c}$ is chosen as a point of application of the contact force $\boldsymbol{f}$, which means that the contact moment has the vertical component η only, where $\boldsymbol{e}_{\mathrm{z}}$ is a unit vector pointing to the positive z direction. By substituting (1a) into (1b), we obtain

$$\dot{\boldsymbol{L}} = \boldsymbol{e}_{\mathrm{z}}\eta - (\boldsymbol{p}-\boldsymbol{c}) \times m(\ddot{\boldsymbol{p}} + \boldsymbol{g}) \tag{2}$$

Now, consider the well-known Linear Inverted Pendulum Mode (LIPM) given by

$$\ddot{\boldsymbol{p}} = \frac{1}{T^2}(\boldsymbol{p}-\boldsymbol{c}) - \boldsymbol{g} \tag{3}$$

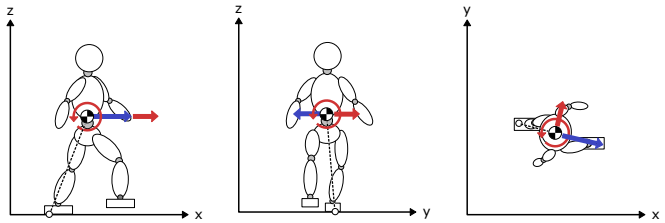

(a) (b) (c)

Fig. 1. Illustration of extra acceleration and resultant recovery moment.

Here, T may generally be time varying, but in this context we consider it to be a positive constant. By substituting (3) into (2), we obtain $\dot{\boldsymbol{L}} = \boldsymbol{e}_{\mathrm{z}}\eta$. This means that as long as the motion of the CoM is governed by the LIPM, the linear dynamics of the CoM and the rotational dynamics of the angular momentum are completely decoupled. This convenient characteristic has been extensively utilized in conventional trajectory generation and balance control methods. From a more general perspective, one can also say that deviation of the CoM from the LIPM causes variation in the angular momentum. More concretely, let us define $\boldsymbol{\delta}$ as extra acceleration of the CoM, with which the CoM motion is now governed by the following equation.

$$\ddot{\boldsymbol{p}} = \frac{1}{T^2}(\boldsymbol{p}-\boldsymbol{c}) - \boldsymbol{g} + \boldsymbol{\delta} \tag{4}$$

By substituting (4) into (2), we obtain

$$\dot{\boldsymbol{L}} = \boldsymbol{e}_{\mathrm{z}}\eta - m(\boldsymbol{p}-\boldsymbol{c}) \times \boldsymbol{\delta} \tag{5}$$

This equation implies, in addition to η (the vertical component of the contact moment), one can utilize $\boldsymbol{\delta}$ to manipulate the angular momentum over a cross product with $\boldsymbol{p}-\boldsymbol{c}$. Note that extra acceleration defined above is closely related to the notion of CMP (centroidal moment pivot); in fact, the CMP is given by $\boldsymbol{c}-T^2\boldsymbol{\delta}$. Although the remaining discussion could be made based on the CMP, we prefer the notion of extra acceleration with which the idea of the proposed rotation stabilization control can be explained more naturally. Extra acceleration $\boldsymbol{\delta}$ can also be seen as deviation from the DCM dynamics. The Divergent Component of Motion (DCM) is defined by $\boldsymbol{\xi} = \boldsymbol{p} + T\dot{\boldsymbol{p}}$. The equation (4) can be rewritten using the DCM as

$$\dot{\boldsymbol{p}} = -\frac{1}{T}(\boldsymbol{p}-\boldsymbol{\xi}) \tag{6}$$

$$\dot{\boldsymbol{\xi}} = \frac{1}{T}(\boldsymbol{\xi}-\boldsymbol{c}) - T\boldsymbol{g} + T\boldsymbol{\delta} \tag{7}$$

Now, let us focus more closely on the cross product term $(\boldsymbol{p}-\boldsymbol{c})\times\boldsymbol{\delta}$ to clarify the relationship between the direction of extra acceleration and that of moment. Let us write $\boldsymbol{r} = \boldsymbol{p}-\boldsymbol{c}$. Then (5) can be rewritten as

$$\dot{L}_{\mathrm{x}} = m(+r_{\mathrm{z}}\delta_{\mathrm{y}} - r_{\mathrm{y}}\delta_{\mathrm{z}}) \tag{8a}$$

$$\dot{L}_{\mathrm{y}} = m(-r_{\mathrm{z}}\delta_{\mathrm{x}} + r_{\mathrm{x}}\delta_{\mathrm{z}}) \tag{8b}$$

$$\dot{L}_{\mathrm{z}} = m(-r_{\mathrm{x}}\delta_{\mathrm{y}} + r_{\mathrm{y}}\delta_{\mathrm{x}}) + \eta \tag{8c}$$

Note that r_{z} expresses the height of the CoM from the ground, while r_{x} and r_{y} express lateral offsets of the CoM from the ZMP. Eqs.(8a) and (8b) indicate that the vertical deviation δ_{z} influences the roll and pitch angular momentum. However, this influence is not so reliable because the moment arms r_{x} and r_{y} are much smaller than r_{z}, and also because the vertical movable range of the DCM (or that of the CoM) is kinematically limited. Moreover, η is useful for controlling L_{z}, but its range is limited by maximum static torsional friction. The relationship between extra acceleration and moment generated by it is summarized as follows.

1) $\boldsymbol{\delta}$ in positive x direction generates negative pitch moment (Fig. 1(a)).
2) $\boldsymbol{\delta}$ in positive y direction generates positive roll moment (Fig. 1(b)).
3) $\boldsymbol{\delta}$ in the perpendicular direction of $(r_{\mathrm{x}}, r_{\mathrm{y}})$ generates positive yaw moment (Fig. 1(c)).

One essential difficulty is that, since cross product with $\boldsymbol{r}$ has rank 2, controlling all three components of $\dot{\boldsymbol{L}}$ using $\boldsymbol{\delta}$ is impossible. In fact, if $\eta = 0$ we have $\boldsymbol{r}^{\mathsf{T}}\dot{\boldsymbol{L}} = 0$. This means that the angular momentum can only be changed in directions that satisfy this one-dimensional constraint.

III. Angular Momentum Regulation Control Based on DCM Modulation

A. Overall Flow of Control System

The diagram of the proposed control system is illustrated in Fig. 2. The control system consists of two main components: rotation stabilizer and continuous step adaptation. They operate in continuous time to react swiftly to disturbances. One of the main advantages of the proposed method is that it requires rotation of the base link as its sole sensory input and estimation of the *real* DCM of the robot is not necessary. The reason why this holds can be explained as follows. Let us assume that the following conditions hold: i) the support foot does not slip, ii) the leg joints are fully actuated and position tracking error is sufficiently small, and iii) errors in kinematic and mass parameters are also sufficiently small. Under these assumptions, the only source of error between the desired and real DCM are base link rotation. Thus, by regulating the base link rotation, the real DCM will naturally converge to its desired value without explicit DCM tracking control.

B. Rotation Stabilization by DCM Modulation

This section describes rotation stabilization by DCM modulation, which is the main contribution of this paper. Let $\boldsymbol{\theta}$ be a vector of Euler angles expressing the rotation of the base link and $\boldsymbol{\omega}$ be the angular velocity of the base link expressed in its local coordinate frame. Under the assumption that the roll and pitch angles are small enough, $\dot{\boldsymbol{\theta}} = \boldsymbol{\omega}$ holds approximately. As discussed earlier, it is impossible to control rotation in all three axes independently by using $\boldsymbol{\delta}$ alone. The basic strategy behind the method described below is to assign higher priority to yaw regulation and encode yaw regulation signal into desired roll/pitch rotation angles. First, desired yaw angular acceleration is determined by a simple PD control law as follows.

$$\dot{\omega}_{\mathrm{des,z}} = K_{\mathrm{P,z}}(\theta_{\mathrm{ref,z}} - \theta_{\mathrm{z}}) + K_{\mathrm{D,z}}(\omega_{\mathrm{ref,z}} - \omega_{\mathrm{z}}) \tag{9}$$

Here, θ_{z} and ω_{z} are measured yaw angle and angular velocity of the base link, while $\theta_{\mathrm{ref},z}$ and $\omega_{\mathrm{ref},z}$ are reference values input to the controller. Moreover, $K_{\mathrm{P},*}$ and $K_{\mathrm{D},*}$ are proportional and differential gains. Next, desired roll/pitch angular accelerations are determined as the least-squares solution satisfying $\boldsymbol{r}^{\mathsf{T}}(I\dot{\boldsymbol{\omega}}_{\mathrm{des}}) = 0$:

$$\begin{aligned}
\dot{\omega}_{\mathrm{des,x}} &= -\frac{I_{\mathrm{z}} r_{\mathrm{x}} r_{\mathrm{z}}}{I_{\mathrm{x}}(r_{\mathrm{x}}^2 + r_{\mathrm{y}}^2)}\dot{\omega}_{\mathrm{des,z}} - k_1\theta_{\mathrm{des,x}} - k_2\omega_{\mathrm{des,x}} \\
\dot{\omega}_{\mathrm{des,y}} &= -\frac{I_{\mathrm{z}} r_{\mathrm{y}} r_{\mathrm{z}}}{I_{\mathrm{y}}(r_{\mathrm{x}}^2 + r_{\mathrm{y}}^2)}\dot{\omega}_{\mathrm{des,z}} - k_1\theta_{\mathrm{des,y}} - k_2\omega_{\mathrm{des,y}}
\end{aligned} \tag{10}$$

Here, we make a simplifying assumption that $\boldsymbol{L} \approx I\boldsymbol{\omega}$ holds, where $I = \mathrm{diag}(I_{\mathrm{x}}, I_{\mathrm{y}}, I_{\mathrm{z}})$ is the nominal inertia around the CoM. Moreover, (10) includes feedback terms with weak gains k_1 and k_2 to prevent desired roll/pitch angles from deviating too much from zero. By integrating (10), desired angle and angular velocity in the roll/pitch directions ($\theta_{\mathrm{des,x}}$, $\theta_{\mathrm{des,y}}$, $\omega_{\mathrm{des,x}}$, and $\omega_{\mathrm{des,y}}$) are updated. Now that desired roll/pitch angles are obtained, desired moment is determined by the following PD control law:

$$\begin{aligned}
\dot{L}_{\mathrm{des,x}} &= I_{\mathrm{x}}(K_{\mathrm{P,x}}(\theta_{\mathrm{des,x}} - \theta_{\mathrm{x}}) + K_{\mathrm{D,x}}(\omega_{\mathrm{des,x}} - \omega_{\mathrm{x}})) \\
\dot{L}_{\mathrm{des,y}} &= I_{\mathrm{y}}(K_{\mathrm{P,y}}(\theta_{\mathrm{des,y}} - \theta_{\mathrm{y}}) + K_{\mathrm{D,y}}(\omega_{\mathrm{des,y}} - \omega_{\mathrm{y}}))
\end{aligned} \tag{11}$$

where θ_{x}, θ_{y}, ω_{x}, and ω_{y} are measured roll/pitch angle and angular velocity of the base link. The DCM modulation signal $\boldsymbol{\delta}$ that generates this moment is given by

$$\begin{aligned}
\delta_{\mathrm{x}} &= \frac{1}{m}\left(-\frac{1}{r_{\mathrm{z}}}\dot{L}_{\mathrm{des,y}}\right), \\
\delta_{\mathrm{y}} &= \frac{1}{m}\left(\frac{1}{r_{\mathrm{z}}}\dot{L}_{\mathrm{des,x}}\right), \\
\delta_{\mathrm{z}} &= 0
\end{aligned} \tag{12}$$

which input to the DCM dynamics equation (7) to update the desired DCM as follows.

$$\dot{\boldsymbol{\xi}}_{\mathrm{des}} = \frac{1}{T}(\boldsymbol{\xi}_{\mathrm{des}} - \boldsymbol{c}_{\mathrm{des}}) - T\boldsymbol{g} + T\boldsymbol{\delta} \tag{13}$$

Let us call this technique *DCM modulation* because the desired DCM is modulated to carry rotation correction signal. Here, the desired ZMP $\boldsymbol{c}_{\mathrm{des}}$ is given by the following feedback law.

$$\boldsymbol{c}_{\mathrm{des}} = \mathrm{proj}_{\mathrm{sup}}(\boldsymbol{c}_{\mathrm{ref}} - K_{\mathrm{dcm}}(\boldsymbol{\xi}_{\mathrm{des}} - \boldsymbol{\xi}_{\mathrm{ref}})) \tag{14}$$

Here, $\boldsymbol{c}_{\mathrm{ref}}$ is the reference ZMP, which is typically located at the center of the support foot, and $\boldsymbol{\xi}_{\mathrm{ref}}$ is the reference DCM given by

$$\boldsymbol{\xi}_{\mathrm{ref}} = \boldsymbol{c}_{\mathrm{ref}} + \exp\left(\frac{t}{T}\right)\boldsymbol{\xi}_{\mathrm{offset}} \tag{15}$$

where t is the elapsed time from the previous support foot exchange and $\boldsymbol{\xi}_{\mathrm{offset}}$ is the nominal DCM offset. Here, K_{dcm} is a feedback gain used to make the desired DCM track the reference DCM. Similar DCM tracking control

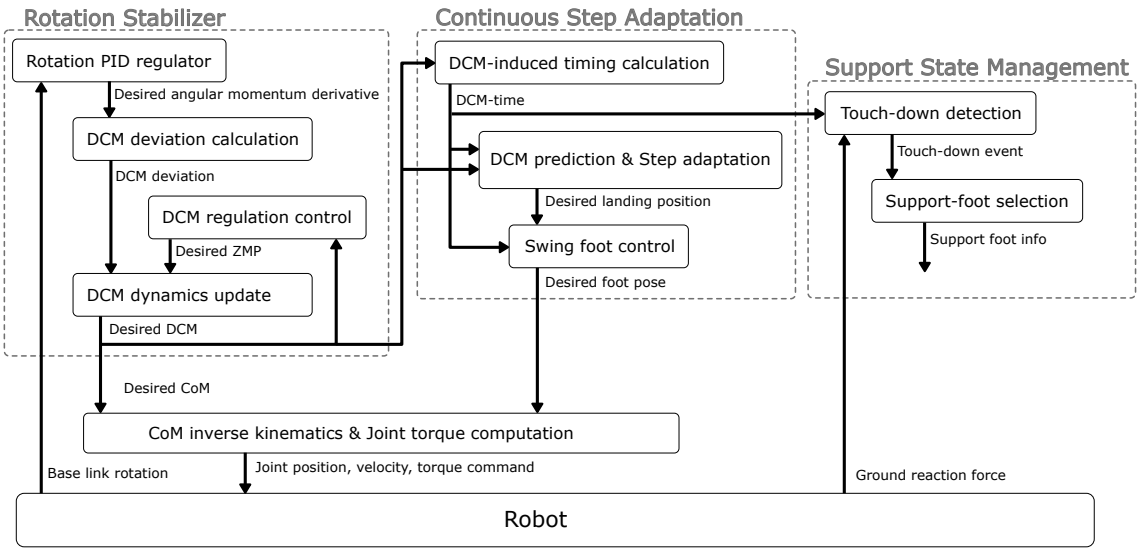

Fig. 2. Control system block diagram

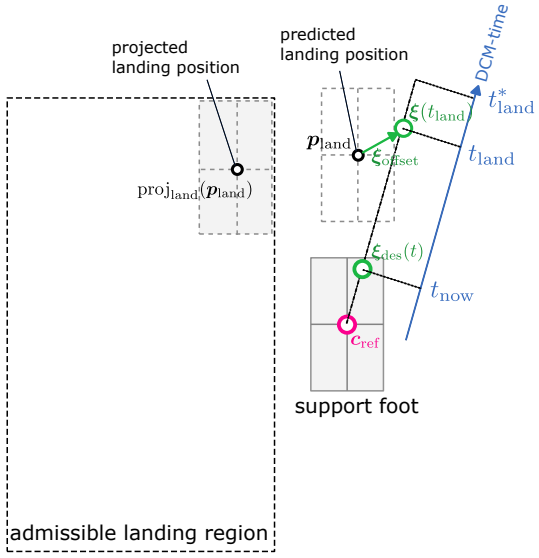

Fig. 3. Step placement and timing adaptation

was used in [28] and [29], although a main difference in our case is that we regulate the desired DCM instead of the real (estimated) one. Moreover, $\mathrm{proj}_{\mathrm{sup}}$ is an operator that projects the desired ZMP inside the support region. Although more sophisticated constraint handling by means of constrained optimization could be considered, we resort to projection for ease of implementation.

C. Step and Timing Adaptation

The step and timing adaptation strategy used in this study is conceptually similar to the work of Khadiv [12]. One notable difference is that a useful notion of DCM-induced time is introduced for natural derivation of timing adaptation. Another difference is that simple projection operation is used instead of constrained optimization to handle restriction of allowable foot placement region. Let t denote elapsed time from the previous support foot exchange. Then the solution of the DCM dynamics is written as

$$\boldsymbol{\xi}(t) = \boldsymbol{c} + \exp\left(\frac{t}{T}\right)(\boldsymbol{\xi}(0) - \boldsymbol{c}). \tag{16}$$

where $\boldsymbol{c}$ denotes the ZMP, which is assume to be fixed during each walking phase. By solving this for t we obtain

$$\begin{aligned} t &= T \log\left(\frac{\|\boldsymbol{\xi}(t) - \boldsymbol{c}\|}{\|\boldsymbol{\xi}(0) - \boldsymbol{c}\|}\right) \\ &= T \log\|\boldsymbol{\xi}(t) - \boldsymbol{c}\| - T \log\|\boldsymbol{\xi}(0) - \boldsymbol{c}\| \\ &= t_{\mathrm{dcm}}(\boldsymbol{\xi}(t) - \boldsymbol{c}) - t_{\mathrm{dcm}}(\boldsymbol{\xi}(0) - \boldsymbol{c}) \end{aligned} \tag{17}$$

Here, $t_{\mathrm{dcm}}(\boldsymbol{\xi} - \boldsymbol{c}) = T \log\|\boldsymbol{\xi} - \boldsymbol{c}\|$ is interpreted as virtual time parametrized by the horizontal distance between the DCM and the ZMP. Let us call it *DCM-induced time* or DCM-time. For later use, let us define $t_{\mathrm{now}}(t) = t_{\mathrm{dcm}}(\boldsymbol{\xi}_{\mathrm{des}}(t) - \boldsymbol{c}_{\mathrm{ref}})$, which gives the DCM-time from the desired DCM at time t. At every instant of support foot exchange, at which t is reset to 0, the timing of the next scheduled support foot exchange is determined as follows.

$$t^*_{\mathrm{land}} = \max(\tau_{\mathrm{nominal}} + t_{\mathrm{dcm}}(\boldsymbol{\xi}_{\mathrm{offset}}),\ \tau_{\mathrm{min}} + t_{\mathrm{now}}(0)) \tag{18}$$

In nominal walking, $\boldsymbol{\xi}_{\mathrm{des}}(0) - \boldsymbol{c}_{\mathrm{ref}} \approx \boldsymbol{\xi}_{\mathrm{offset}}$ holds. In this case, t^*_{land} is scheduled τ_{nominal} (nominal step duration) ahead of t_{now}. When walking is disturbed, however, t^*_{land} calculated this way could be too close or even smaller than $t_{\mathrm{now}}(0)$. To avoid this situation, t^*_{land} is set at least τ_{min} (minimum step duration) ahead of the DCM-time at support foot exchange. landing time is continuously adjusted during the swing phase as illustrated in Fig. 3 to take limitation of foot placement into account. Let $t_{\mathrm{land}} \in [t_{\mathrm{now}}(t), t^*_{\mathrm{land}}]$ be adjusted landing time. Given t_{land}, remaining time to landing is given by

$$\tau_{\mathrm{ttl}} = t_{\mathrm{land}} - t_{\mathrm{now}}(t). \tag{19}$$

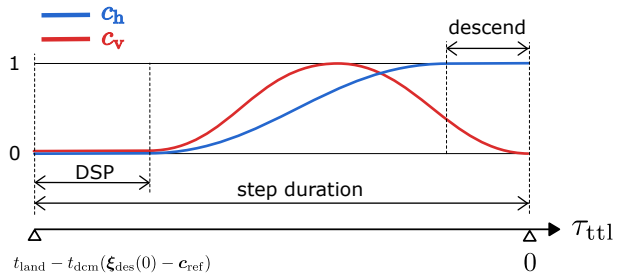

Fig. 4. Cycloid basis functions of swing foot trajectory

Predicted DCM at landing can be calculated as follows.

$$\boldsymbol{\xi}(t_{\text{land}}) = \boldsymbol{c}_{\text{ref}} + \exp\left(\frac{\tau_{\text{ttl}}}{T}\right)(\boldsymbol{\xi}_{\text{des}}(t) - \boldsymbol{c}_{\text{ref}}) \tag{20}$$

To achieve a predefined DCM offset right after landing, the landing position of the swing foot is given by

$$\boldsymbol{p}_{\text{land}} = \boldsymbol{\xi}(t_{\text{land}}) - R_{\text{z}}(\theta_{\text{land}})\boldsymbol{\xi}_{\text{offset}} \tag{21}$$

where R_{z} denotes a rotation matrix about the z axis. Finally, landing position is projected inside admissible landing region. Based on the procedure described above, the adjusted landing time is given by the solution of the following one-dimensional optimization problem:

$$\begin{aligned}\min_{t_{\text{land}} \in [t_{\text{now}}(t), t^*_{\text{land}}]} \; & w\|\boldsymbol{p}_{\text{land}} - \text{proj}_{\text{land}}(\boldsymbol{p}_{\text{land}})\| \\ & + |t_{\text{land}} - t^*_{\text{land}}|\end{aligned} \tag{22}$$

Here, w is a weight that prioritizes landing position error over timing error.

D. Swing foot control

The swing foot movement is parametrized DCM-time instead of real time. In this manner, the movement of the swing foot is synchronized with that of the desired DCM. More concretely, the position and turning angle of the swing foot is expressed as follows.

$$\boldsymbol{p}_{\text{swing}}(\tau_{\text{ttl}}) = \boldsymbol{p}_{\text{lift}} + c_{\text{h}}(\tau_{\text{ttl}})(\boldsymbol{p}_{\text{land}} - \boldsymbol{p}_{\text{lift}}) + c_{\text{v}}(\tau_{\text{ttl}})h_{\text{swing}} \tag{23}$$

$$\theta_{\text{swing}}(\tau_{\text{ttl}}) = \theta_{\text{lift}} + c_{\text{h}}(\tau_{\text{ttl}})(\theta_{\text{land}} - \theta_{\text{lift}}) \tag{24}$$

Here, $(\boldsymbol{p}_{\text{swing}}, \theta_{\text{swing}})$ denote the position and yaw angle of the swing foot, and τ_{ttl} is given by (19). Similarly, $(\boldsymbol{p}_{\text{lift}}, \theta_{\text{lift}})$ and $(\boldsymbol{p}_{\text{land}}, \theta_{\text{land}})$ denote the swing foot pose at lift-off and landing, respectively, and h_{swing} is the swing height. Moreover, c_{h} and c_{v} are sigmoidal functions illustrated in Fig. 4. The first part of the period is specified as the double-support phase (DSP) during which both c_{h} and c_{v} are zero. During the last part, on the other hand, c_{h} is fixed to 1, meaning that the horiontal and turning movement completes earlier than the vertical movement. This helps to reduce the risk of ground-scuffing right before touch down.

TABLE I
TABLE OF CONTROL PARAMETERS

	roll	pitch	yaw
K_{P}	400	400	10
K_{I}	120	120	0
K_{D}	40	40	10
K_{dcm}	2		

τ_{nominal}	0.45
τ_{min}	0.30
h_{swing}	0.10

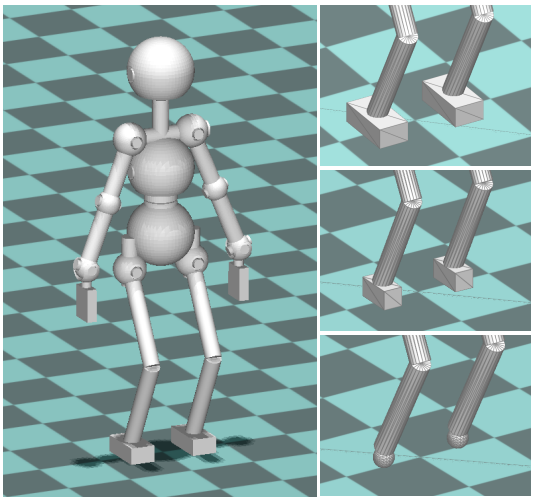

Fig. 5. Robot model used for simulation. Entire view (left) and different foot geometries (right, from top to bottom, large, small, and point).

IV. Simulation Results

A. Common Setup

The performance of the proposed controller was tested in dynamical simulation. See the attached video for better visualization of simulation results. A C++ implementation of the proposed controller is publicly available in an open-source software library `vnoid` [1]. Choreonoid with AIST simulator [30] was used for testing. A 30-DoF humanoid robot model shown in Fig. 5 was used for simulation. Although its appearance is unrealistic, its kinematic parameters and mass distribution resemble those of real humanoids. It has two DoFs in the torso, two in the neck, seven in each arm, and six in each leg. The total mass is $m = 43$kg. Each arm and each leg weighs 4.5kg and 5.0kg, respectively. The nominal inertia was set as $(I_{\text{x}}, I_{\text{y}}, I_{\text{z}}) = (2.5, 2.5, 0.2)$kg·m^2. These values are based on numerically computed composite rigid-body inertia of the robot in a neutral pose. A rate sensor (a gyroscope) and an accelerometer are attached to the base link to measure its three-axis rotation. A 6-axis force sensor is attached to each foot, although it is used for touch-down detection only. The nominal CoM height was set as $h = 0.7$m, and the constant T was set as $T = \sqrt{h/g} \approx 0.27$, where $g \approx 9.8$ is the gravitational acceleration. The controller parameters are set as shown in Table I.

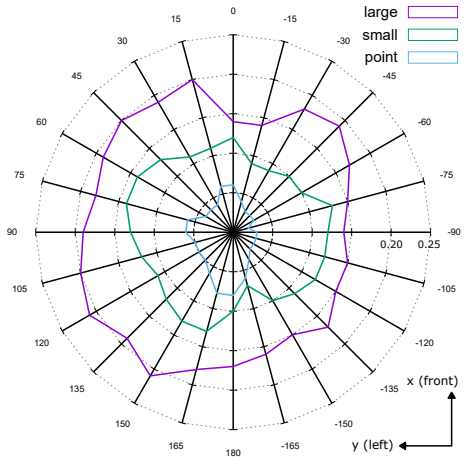

(a)

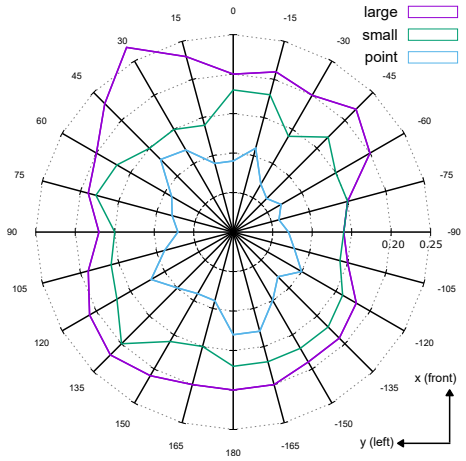

(b)

Fig. 6. Maximum tolerable disturbance in different directions and timing. Disturbance was applied in the beginning of the right support phase (a), and in the middle of the right support phase (b). The magnitude of disturbance is expressed by equivalent DCM shift [m].

B. Evaluation of robustness under disturbances

The robustness of the proposed controller against impulsive disturbances was evaluated. While the robot stepped in place, horizontal force with varying magnitude and direction was applied to the CoM at controlled timing during the right support phase for a fixed duration of 50ms. For each direction, the maximum magnitude of disturbance after which the robot could continue stepping without falling down was measured. The result is summarized in a radar chart shown in Fig. 6(a),(b). In the figure, the magnitude of disturbance is expressed by the equivalent instantaneous shift of the DCM in meters. The test was conducted using different foot geometries: large foot (a box-shaped foot with a dimension of $X \times Y = 0.15\text{m} \times 0.075\text{m}$, small foot ($X \times Y = 0.1\text{m} \times 0.05\text{m}$), and point foot (a sphere-shaped foot with a radius of 0.025m). With small foot support area, angular velocity in the yaw direction was likely to be

[1]https://github.com/ytazz/vnoid

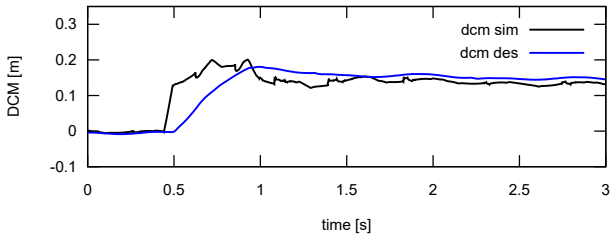

Fig. 7. Response of real DCM (black) and desired DCM (blue) after forward impulsive disturbance.

generated as a result of disturbance injection. For this reason, even small difference in the direction of disturbance resulted in notable difference in tolerable disturbance magnitude. The result shown above is comparable to similar benchmark results reported in [12] and [13].

Figure 7 shows responses of the real DCM computed from states directly obtained from the simulator and the desired DCM computed inside the controller when a forward impulsive push with an equivalent DCM shift of 0.2m was applied. While the real DCM changed instantaneously after disturbance injection, the desired DCM changed linearly at approximately 0.5m/s. Different combination of gains of the rotation stabilization control (11) had little effect in the rate of change. This result indicates that the proposed controller has certain limitation in its responsiveness to impulsive disturbances due to the fact that it updates the desired DCM in response to inclination of the base link. The responding speed could be improved by taking horizontal acceleration of the base link into account.

C. Yaw-regulated walking of a point-foot robot

For demonstration of yaw control without using ground reaction moment, the proposed controller was tested with a robot model with point foot. In this setup, the torsional friction coefficient is practically zero, meaning that the robot must maintain balance based purely on DCM modulation and step adaptation. The robot was commanded to walk along a polygonal reference path composed of 1m straight line segments (0.2m maximum stride length) and 120deg corners (8.6deg maximum turning angle per step). As shown in Fig. 8(a), the heading direction of the robot was completely out of control without yaw regulation although the robot did not fall down. By contrast, with yaw regulation turned on, the robot could precisely track the reference path as shown in Fig. 8(b). A certain degree of tracking error was inevitable because no absolute position feedback was implemented. Plots of desired and simulated base link rotation with yaw regulation control are shown in Fig. 9. One can observe that periodic variation of desired roll/pitch angles was generated to regulate the yaw angle during forward walking, whereas pitch angle variation was mainly generated to create yaw moment required for turning on the spot. Although this result may have little direct impact on practical application, it is considered to have notable theoretical value because no similar result has been reported in the literature.

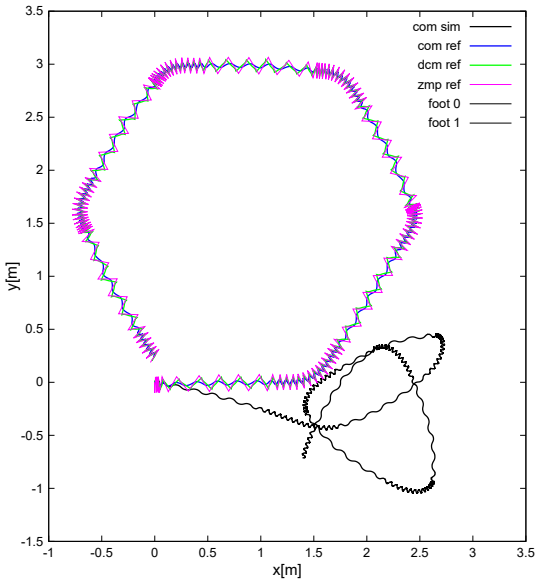

(a) without yaw regulation

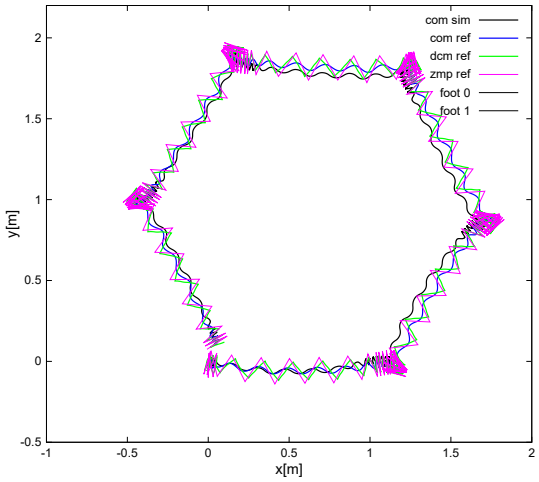

(b) with yaw regulation

Fig. 8. Trajectory of a point-foot robot walking along a polygonal path. Simulated CoM (black), desired CoM (blue), desired DCM (green), desired ZMP (magenta).

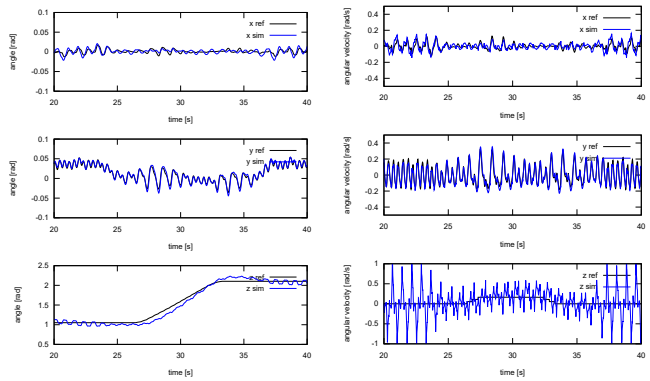

Fig. 9. Time profile of base link rotation from $t = 20$[s] to $t = 40$[s]. Angle (left) and angular velocity (right). Desired value (black) and measured value (blue).

V. Conclusion

This paper presented a simple walking controller that can stabilize three-axis rotation without relying on ground reaction moment. One shortcoming of the presented controller, which encodes desired yaw angular acceleration into desired roll/pitch rotation, is that the yaw feedback gain cannot be set very high for fear of disrupting the stability of walking. Predictive control methods could be used to control rotation along three axes in a more unified manner.

Acknowledgement

This work was supported by JSPS KAKENHI Grant Number JP24K03017.

[1] T. Egle, Y. Yan, D. Lee, and C. Ott. Enhancing model-based step adaptation for push recovery through reinforcement learning of step timing and region. In *2024 IEEE-RAS 23rd International Conference on Humanoid Robots (Humanoids)*, pages 165–172, 2024.

[2] T. Komura, H. Leung, S. Kudoh, and J. Kuffner. A feedback controller for biped humanoids that can counteract large perturbations during gait. In *Proceedings of the 2005 IEEE International Conference on Robotics and Automation*, pages 1989–1995, 2005.

[3] A. Hofmann, M. Popovic, and H. Herr. Exploiting angular momentum to enhance bipedal center-of-mass control. In *2009 IEEE International Conference on Robotics and Automation*, pages 4423–4429, 2009.

[4] S.-H. Lee and A. Goswami. A momentum-based balance controller for humanoid robots on non-level and non-stationary ground. *Autonomous Robots*:399–414, 2012.

[5] K. Guan, K. Yamamoto, and Y. Nakamura. Push recovery by angular momentum control during 3d bipedal walking based on virtual-mass-ellipsoid inverted pendulum model. In *2019 IEEE-RAS 19th International Conference on Humanoid Robots (Humanoids)*, pages 120–125, 2019.

[6] H. Jeong, I. Lee, J. Oh, K. K. Lee, and J.-H. Oh. A robust walking controller based on online optimization of ankle, hip, and stepping strategies. *IEEE Transactions on Robotics*, 35(6):1367–1386, 2019.

[7] J. Ding, C. Zhou, S. Xin, X. Xiao, and N. Tsagarakis. Nonlinear model predictive control for robust bipedal locomotion: exploring angular momentum and com height changes. *Advanced Robotics*, 35(18):1079–1097, 2021.

[8] J. Choe, J.-H. Kim, S. Hong, J. Lee, and H.-W. Park. Seamless reaction strategy for bipedal locomotion exploiting real-time nonlinear model predictive control. *IEEE Robotics and Automation Letters*, 8(8):5031–5038, 2023.

[9] G. Park, J. H. Kim, J. Jo, and Y. Oh. Lyapunov-based approach to reactive step generation for push recovery of biped robots via hybrid tracking control of dcm. In *2020 IEEE/RSJ International Conference on Intelligent Robots and Systems (IROS)*, pages 3504–3509, 2020.

[10] X. Xiong, Y. Chen, and A. D. Ames. Robust disturbance rejection for robotic bipedal walking: system-level-synthesis with step-to-step dynamics approximation. In *2021 60th IEEE Conference on Decision and Control (CDC)*, pages 697–704, 2021.

[11] G. Gibson, O. Dosunmu-Ogunbi, Y. Gong, and J. Grizzle. Terrain-adaptive, alip-based bipedal locomotion controller via model predictive control and virtual constraints. In *2022 IEEE/RSJ International Conference on Intelligent Robots and Systems (IROS)*, pages 6724–6731, 2022.

[12] M. Khadiv, A. Herzog, S. A. A. Moosavian, and L. Righetti. Walking control based on step timing adaptation. *IEEE Transactions on Robotics*, 36(3):629–643, 2020.

[13] G. Mesesan, J. Englsberger, and C. Ott. Online dcm trajectory adaptation for push and stumble recovery during humanoid locomotion. In *2021 IEEE International Conference on Robotics and Automation (ICRA)*, pages 12780–12786, 2021.

[14] L. Han, X. Chen, Z. Yu, J. Zhang, Z. Gao, and Q. Huang. Enhancing speed recovery rapidity in bipedal walking with limited foot area us-

ing dcm predictions. *Expert Systems with Applications*, 250:123858, 2024. ISSN: 0957-4174.
[15] R. Griffin, J. Foster, S. Fasano, B. Shrewsbury, and S. Bertrand. Reachability aware capture regions with time adjustment and cross-over for step recovery. In *2023 IEEE-RAS 22nd International Conference on Humanoid Robots (Humanoids)*, pages 1–8, 2023.
[16] Y. Kojio, Y. Omori, K. Kojima, F. Sugai, Y. Kakiuchi, K. Okada, and M. Inaba. Footstep modification including step time and angular momentum under disturbances on sparse footholds. *IEEE Robotics and Automation Letters*, 5(3):4907–4914, 2020.
[17] T. Koolen, M. Posa, and R. Tedrake. Balance control using center of mass height variation: limitations imposed by unilateral contact. In *2016 IEEE-RAS 16th International Conference on Humanoid Robots (Humanoids)*, pages 8–15, 2016.
[18] S. Caron and B. Mallein. Balance control using both zmp and com height variations: a convex boundedness approach. In *2018 IEEE International Conference on Robotics and Automation (ICRA)*, pages 1779–1784, 2018.
[19] S. Caron, A. Escande, L. Lanari, and B. Mallein. Capturability-based pattern generation for walking with variable height. *IEEE Transactions on Robotics*, 36(2):517–536, 2020.
[20] S. Caron. Biped stabilization by linear feedback of the variable-height inverted pendulum model. In *2020 IEEE International Conference on Robotics and Automation (ICRA)*, pages 9782–9788, 2020.
[21] M. B. Popovic, A. Goswami, and H. Herr. Ground reference points in legged locomotion: definitions, biological trajectories and control implications. *The International Journal of Robotics Research*, 24(12):1013–1032, 2005.
[22] J. Englsberger, C. Ott, and A. Albu-Shäffer. Three-dimensional bipedal walking control based on divergent component of motion. *IEEE Trans. Robotics*, 31(2):355–368, 2015.
[23] T. Takenaka, T. Matsumoto, and T. Yoshiike. Real time motion generation and control for biped robot -3rd report: dynamics error compensation-. In *2009 IEEE/RSJ International Conference on Intelligent Robots and Systems*, pages 1594–1600, 2009.
[24] J. Englsberger and C. Ott. Integration of vertical com motion and angular momentum in an extended capture point tracking controller for bipedal walking. In *2012 12th IEEE-RAS International Conference on Humanoid Robots (Humanoids 2012)*, pages 183–189, 2012.
[25] R. Schuller, G. Mesesan, J. Englsberger, J. Lee, and C. Ott. Online learning of centroidal angular momentum towards enhancing dcm-based locomotion. In *2022 International Conference on Robotics and Automation (ICRA)*, pages 10442–10448, 2022.
[26] K. Nagasaka. The whole-body motion generation of humanoid robot using dynamics filter. PhD Thesis, University of Tokyo, 2000. in Japanese.
[27] T. Takenaka, T. Matsumoto, T. Yoshiike, T. Hasegawa, S. Shirokura, H. Kaneko, and A. Orita. Real time motion generation and control for biped robot -4th report: integrated balance control-. In *2009 IEEE/RSJ International Conference on Intelligent Robots and Systems*, pages 1601–1608, 2009.
[28] H. Jeong, I. Lee, O. Sim, K. Lee, and J.-H. Oh. A robust walking controller optimizing step position and step time that exploit advantages of footed robot. *Robotics and Autonomous Systems*, 113:10–22, 2019. ISSN: 0921-8890.
[29] Y. Kojio, Y. Ishiguro, K.-N.-K. Nguyen, F. Sugai, Y. Kakiuchi, K. Okada, and M. Inaba. Unified balance control for biped robots including modification of footsteps with angular momentum and falling detection based on capturability. In *2019 IEEE/RSJ International Conference on Intelligent Robots and Systems (IROS)*, pages 497–504, 2019.
[30] S. Nakaoka. Choreonoid: extensible virtual robot environment built on an integrated gui framework. In *2012 IEEE/SICE International Symposium on System Integration (SII)*, pages 79–85, 2012.

APPENDIX

A. Determining DCM Offset Based on Gait Parameters

As illustrated in Fig. 10, let d_x, d_y, w, ϕ, and τ be stride length, lateral sway per step, lateral spacing of the feet, turning angle per step, and nominal step duration, respectively. Define a coordinate frame in which the right foot at the 0-th step is located at its origin. Moreover, let the

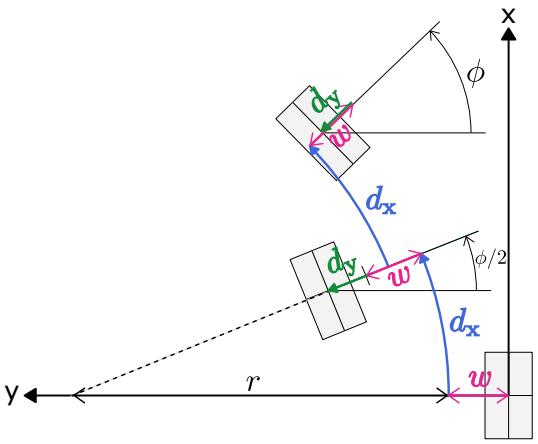

Fig. 10. DCM offset of stationary walking including swaying and turning

position of the next left and right foot placement be $\boldsymbol{p}_1$ and $\boldsymbol{p}_2$, respectively. From the figure, we have

$$\begin{aligned}\boldsymbol{p}_1 &= \begin{bmatrix}0\\ r+w/2\end{bmatrix} + R_\mathrm{z}(\phi/2)\begin{bmatrix}0\\ -r+w/2+d_\mathrm{y}/2\end{bmatrix}\\ \boldsymbol{p}_2 &= \boldsymbol{p}_1 + R_\mathrm{z}(\phi/2)\begin{bmatrix}0\\ r-w/2\end{bmatrix} + R_\mathrm{z}(\phi)\begin{bmatrix}0\\ -r-w/2+d_\mathrm{y}/2\end{bmatrix}\end{aligned} \tag{25}$$

where $r = d_\mathrm{x}/\phi$. From the stationarity of the gait, the DCM at the beginning of the 0-th step and the 2nd step (both right support) relative to the respective support foot must be the same. Let this be $\boldsymbol{\xi}_\mathrm{r}$. Moreover, let the DCM offset of the 1st step (left support) be $\boldsymbol{\xi}_\mathrm{l}$. From the DCM dynamics, we have

$$\begin{aligned}\boldsymbol{p}_1 &= \alpha\boldsymbol{\xi}_\mathrm{r} - R_\mathrm{z}(\phi/2)\boldsymbol{\xi}_\mathrm{l},\\ \boldsymbol{p}_2 &= \alpha\boldsymbol{\xi}_\mathrm{r} + (\alpha-1)R_\mathrm{z}(\phi/2)\boldsymbol{\xi}_\mathrm{l} - R_\mathrm{z}(\phi)\boldsymbol{\xi}_\mathrm{r}.\end{aligned} \tag{26}$$

where $\alpha = \exp(\tau/T)$. Solving these for the DCM offsets gives

$$\begin{aligned}\boldsymbol{\xi}_\mathrm{r} &= (\alpha^2 I - R_\mathrm{z}(\phi))^{-1}((\alpha-1)\boldsymbol{p}_1 + \boldsymbol{p}_2),\\ \boldsymbol{\xi}_\mathrm{l} &= R_\mathrm{z}(\phi/2)^\mathsf{T}(\alpha\boldsymbol{\xi}_\mathrm{r} - \boldsymbol{p}_1)\end{aligned} \tag{27}$$

where I is the 2×2 identity matrix. Substitute (25) into (27) to obtain the DCM offsets.